Energies **2015**, *8*, 9584-9593; doi:10.3390/en8099584

OPEN ACCESS

energies

ISSN 1996-1073

www.mdpi.com/journal/energies

Article

Electrochemical Properties for Co-Doped Pyrite with High Conductivity

Yongchao Liu and Shengping Wang *

Faculty of Materials Science and Chemistry, China University of Geosciences, Wuhan 430074, China; E-Mail: yongcliu@163.com

* Author to whom correspondence should be addressed; E-Mail: spwang@cug.edu.cn; Tel.: +86-27-6788-3731.

Academic Editor: Sheng S. Zhang

Received: 27 June 2015 / Accepted: 26 August 2015 / Published: 2 September 2015

Abstract: In this paper, the hydrothermal method was adopted to synthesize nanostructure Co-doped pyrite (FeS_2). The structural properties and morphology of the synthesized materials were characterized using X-ray diffraction (XRD) and scanning electron microscopy (SEM), respectively. Co in the crystal lattice of FeS_2 could change the growth rate of different crystal planes of the crystal particles, which resulted in various polyhedrons with clear faces and sharp outlines. In addition, the electrochemical performance of the doping pyrite in Li/FeS_2 batteries was evaluated using the galvanostatic discharge test, cyclic voltammetry and electrochemical impedance spectroscopy. The results showed that the discharge capacity of the doped material (801.8 $mAh \cdot g^{-1}$) with a doping ratio of 7% was significantly higher than that of the original FeS_2 (574.6 $mAh \cdot g^{-1}$) because of the enhanced conductivity. Therefore, the doping method is potentially effective for improving the electrochemical performance of FeS_2.

Keywords: pyrite; lithium iron disulfide battery; Co doping; electrochemical performances

1. Introduction

During the past two decades, transition-metal sulfides have received a great deal of interest because of their wide range of applications [1–3]. In particular, pyrite (FeS_2) has attracted a good proportion of research attention and has long been considered one of the most attractive cathode materials for lithium

secondary batteries because of its high theoretic capacity (890 $mAh \cdot g^{-1}$), low environmental pollution and affordable cost [4–8]. It is well known that FeS_2 is a semiconductor with low conductivity, which may result in poor electrical contact between the active particles and the conductive agent and low electrochemical reaction rate during cycling. To overcome the problem, some effective methods were used to improve its conductivity, such as chemical synthesis, doping and conductive polymer coating. The FeS_2 powder with small diameter and homogeneous distribution can be obtained using chemical synthesis methods, such as hydrothermal [9], sol-gel [10], and electrochemical precipitation [11]. Zhang *et al*. [12] obtained coated FeS_2 powder with polyaniline, and the electronic conductivity of the resultant powders was improved. Choi *et al*. [13] achieved modified FeS_2 material by adding Fe powder, and its electrochemical performance was significantly improved. However, the chemical synthesis and conductive polymer coating require a high temperature and complex operation, and, intrinsically, these methods did not improve the electronic conductivity of the crystal. Furthermore, the electronic characteristics can be tuned by modifying their electron filling with doping [14].

In the unit cell, the Fe atom occupies the corner and center of face of the polyhedron, and the S atoms are located at midpoint of the edge, where the octahedral is comprised of one Fe atom and six S atoms. Meanwhile, three Fe atoms and two S atoms are linked to constitute a tetrahedral coordination [15]. Based on this structure, Lehner *et al*. [16] found that (according to crystal field theory) Co and Fe were similar, where the low-spin Fe^{2+} is $(t2g)^6$ and low-spin Co^{2+} is $(t2g)^6(eg)^1$. According to the molecular orbital theory, both can form three π orbitals with the empty sulfur d orbitals. In the case of Co, the extra $(eg)^1$ electron is free to enter the conduction band as a charge carrier in the antibonding $CoS_2\sigma^*$ orbital, which is a result of the stabilization energy. The energy of this orbital is just below and overlapping the $FeS_2\sigma^*$ orbital energy range [17,18]. The energy decrease of the $(t2g)^6$ electrons compensates for the energy required to promote the $(eg)^1$ electron into the antibonding σ* orbital, assuming that one Co atom contributes one charge carrier and replaces the Fe atom in the pyrite unit cell. In addition, according to reports, CoS_2 is also a high-activity candidate electrode material for lithium-ion batteries [19], solar cells [20], and electrocatalysis [21].

In the present work, FeS_2 was obtained using simple hydrothermal synthesis. $CoCl_2 \cdot 6H_2O$ was considered a doping reagent, which was added to raw FeS_2 material, which was intended to immigrate into the FeS_2 lattice and substitute for Fe or the vacancies. As a result, the electrochemical performance of Co-doped FeS_2 for Li/FeS_2 batteries was improved. The highest initial discharge capacity of Co-doped FeS_2 was 801.8 $mAh \cdot g^{-1}$, which was significantly higher than that of the original FeS_2 (574.6 $mAh \cdot g^{-1}$).

2. Experimental Section

2.1. Preparation of the Samples

All chemical reagents (analytical grade) were used as received without further purification. Polyvinylpyrrolidone (PVP) and polyvinyl alcohol (PVA, the Degree of Polymerization: 1750 ± 50) solutions (3 wt%) were purchased from Sinopharm Chemical Reagent Co., Ltd. (Shanghai, China).

First, 0.60 g PVP was dissolved in a mixed solution of 10 mL distilled water and 25 mL PVA. Then, 0.009 mol of ferrous chloride heptahydrate ($FeCl_2 \cdot 7H_2O$) and a specific amount of Cobalt(II)

chloride hexahydrate ($CoCl_2 \cdot 6H_2O$) were added to this solution under constant stirring to form a homogeneous solution. Subsequently, 39 mL 0.75 $mol \cdot L^{-1}$ sodium hydroxide (NaOH) was dropwise added into the solution. Finally, 1.80 g sulfur powder (S) was added to the solution under magnetic stirring for 30 min. The mixture was sealed in a Teflon-lined stainless steel autoclave (80% filled) and heat-treated at 180 °C for 12 h. When the reaction finished, a black powder was obtained by centrifugation, which was rinsed with ethanol and distilled water three times and subsequently dried in an oven at 80 °C. This as-prepared powder was FeS_2. The powder was carried into a horizontal tube furnace and heat-treated under a flow of the high-purity Ar for 6 h at 400 °C (noted as DH-0). Meanwhile, FeS_2 doped with various Co concentrations (3 wt%, 5 wt%, 7 wt%, 9 wt% and 11 wt%) was marked as DH-3, DH-5, DH-7, DH-9 and DH-11, respectively. The actual Co concentrations are determined using wavelength dispersive X-ray fluorescence (WD-XRF).

2.2. Materials Characterization

The X-ray diffraction (XRD) patterns of the samples were obtained using a Bruker/D8-FOCUS diffractometer at a voltage of 40 kV and a current of 40 mA, with Cu Kα radiation (0.1542 nm). The morphology was carried out with a Hitachi/SU8010 high-resolution field emission scanning electron microscope (SEM). In addition, the actual Co concentrations of all Co-doped FeS_2 samples was determined using a PANalytical/AxiosMax wavelength dispersive X-ray fluorescence spectrometer and the resistivity of all Co-doped FeS_2 samples was measured with a Radiant/RT66B ferroelectric tester, respectively.

2.3. Electrochemical Measurement

Electrochemical experiments were performed using coin-type cells, which were assembled in an argon-filled glovebox with lithium foil as the anode electrode at room temperature. The cathode was prepared by mixing 60 wt% active materials, 25 wt% carbon black, and 15 wt% polyvinylidene difluoride (PVDF), which were added in N-methyl-2-pyrrolidone (NMP). Subsequently, the slurry was pasted onto the aluminum foil and allowed to dry at 65 °C in air. The resulting electrode contained ~6.6 mg of the active material, which is a thickness of 250 μm, a diameter of 15 mm, and an apparent area of ~1.766 cm^2. The Celgard 2400 membrane was used as the separator, and 1 M $LiClO_4$:PC:DME (volume ratio of PC to DME is 1:1) was used as the electrolyte.

The discharge measurements were operated at a voltage range of 1.0–2.5 V on a Arbin/BT2000 battery testing instrument at 0.2 $mA \cdot cm^{-2}$ (53.5 $mA \cdot g^{-1}$). Electrochemical impedance spectroscopy (EIS) was performed on a Bio-Logic/VMP3 electrochemical workstation over a frequency range of 100 kHz to 10 mHz with an amplitude of 5 mV.

3. Results and Discussion

The WD-XRF quantitative analysis results indicates the Co concentration of DH-0, DH-3, DH-5, DH-7, DH-9, and DH-11 are 0 wt%, 2.93 wt%, 4.75 wt%, 6.31 wt%, 8.17 wt%, and 10.03 wt%, respectively. Meanwhile, as shown in Figure 1, the characteristic peaks of all samples are indexed as cubic pyrite FeS_2 (JCPDS No. 71-0053), which indicates that the crystal structure of FeS_2 was not

changed with Co doping. The patterns of the heat-treated FeS_2 and doped FeS_2 show a tiny peak at 44.06°, which is attributed to pyrrhotite (Fe_7S_8), which formed during the thermal process. Meanwhile, the peak intensity of DH-9 and DH-11 significantly decreased, which suggests that Co doping could suppress the formation of Fe_7S_8.

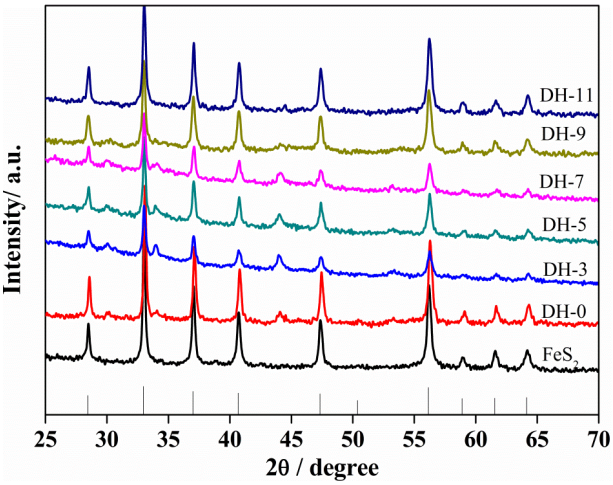

Figure 1. XRD patterns of the samples.

The resistivity of DH-0, DH-3, DH-5, DH-7, DH-9 and DH-11 is 1.25×10^{-2}, 3.72×10^{-2}, 1.02×10^{-2}, 8.65×10^{-3}, 4.32×10^{-3} and 1.97×10^{-4} Ω·cm, respectively. This result indicates that the resistivity of Co-doped FeS_2 samples decreased gradually with the increase of Co concentration, which is in accordance with the results reported by Oertel *et al.* [22] The carrier concentration of FeS_2 increased and its conductive type transformed from p-type to n-type with the doping of Co cation.

In addition, as shown in Figure 2, the SEM pictures verify that DH-7 shows significant face and sharp outline of the polyhedrons, which indicates that the Co doping could change the growth rate of different crystal planes. Although the Co doping could not change the crystal structure of FeS_2, it could change the morphology of the doped FeS_2 samples.

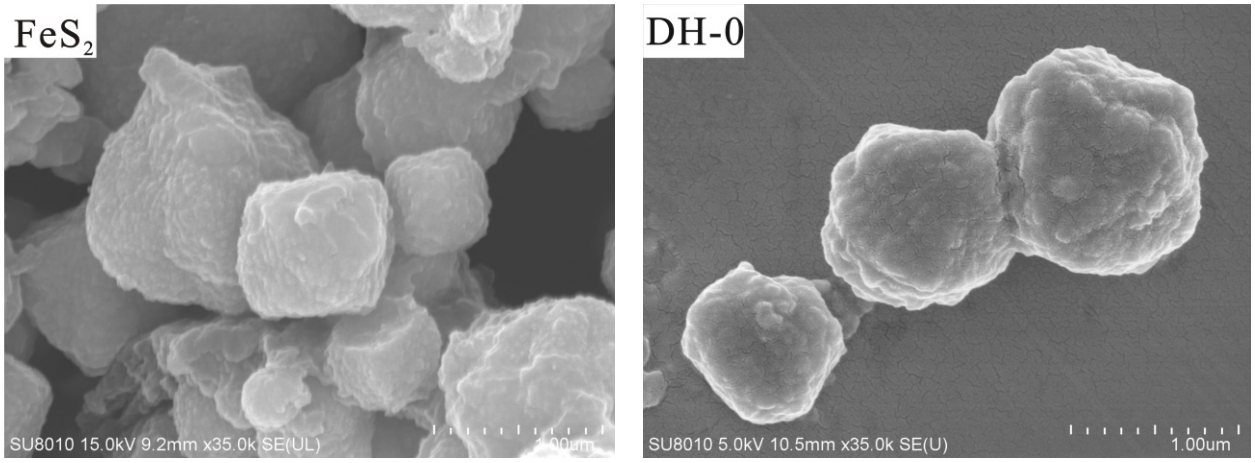

(a) **(b)**

Figure 2. *Cont.*

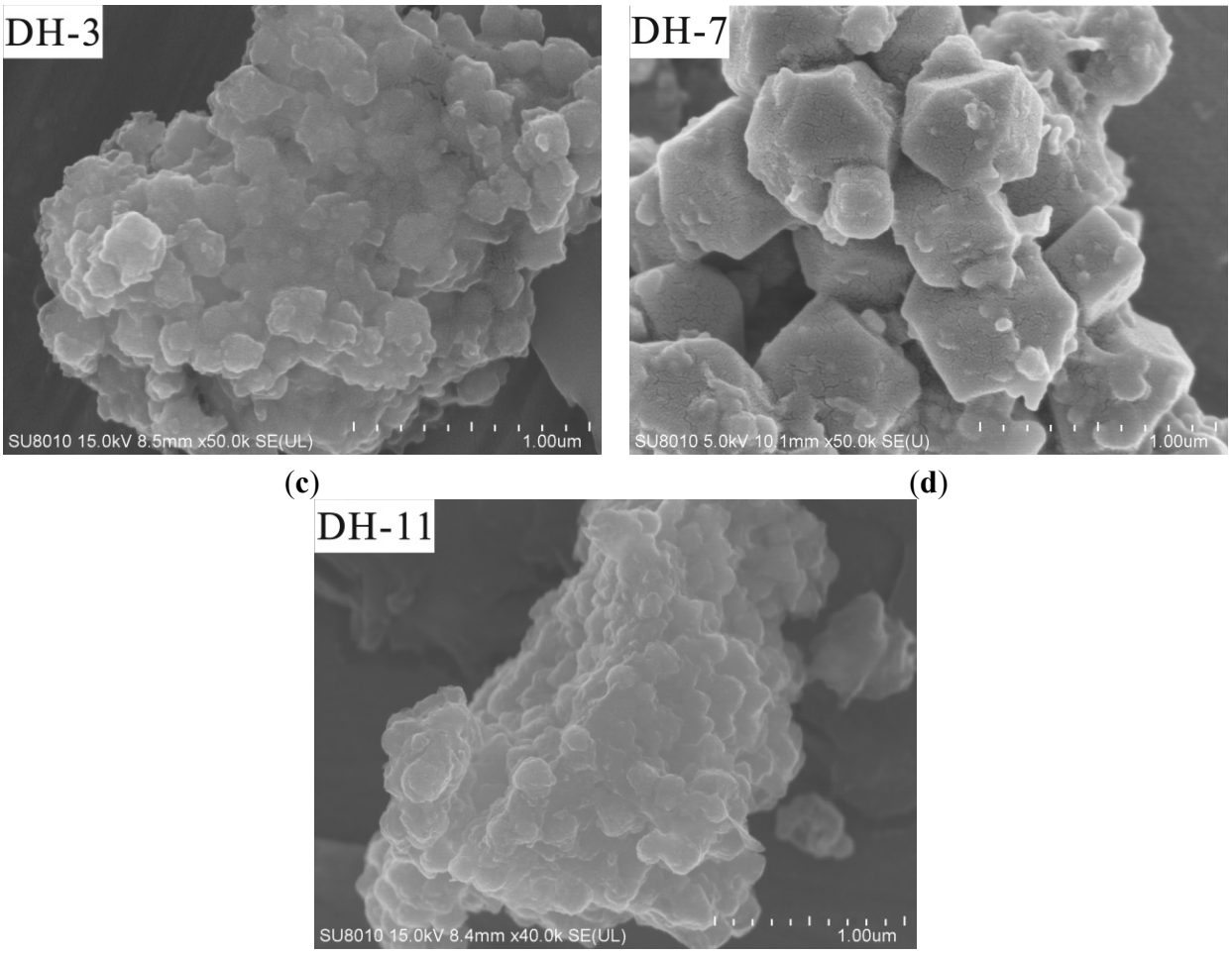

Figure 2. SEM images of the samples. (**a**) FeS_2, (**b**) DH-0, (**c**) DH-3, (**d**) DH-7 and (**e**) DH-11.

As shown in Figure 3, the Co-doped samples have higher initial discharge capacities than FeS_2, particularly DH-7, which reached 801.8 $mAh \cdot g^{-1}$. Furthermore, because of the lowest charge transfer resistance and highest Li^+ diffusion rate (Table 1), DH-7 shows the best electrochemical performance among all doped samples. This result indicates that the electrochemical performance of FeS_2 can be improved by Co doping, and the optimum concentration of doping is not the highest one. Compared with the non-heat-treated FeS_2, the electrochemical properties of the samples DH-0 were improved. This result is mainly related to two reasons. First, the impurity was removed to some extent after the calcination, which made the sample structure more suitable for electrochemical reaction [23]. Second, the surface of the heat-treated material was changed and might generate adsorption sites [24], which facilitated the absorption of Li^+ and improved the electrochemical performance.

The 1st discharge curves of all samples in Figure 4a reveal one discharge plateau and two charge plateaus, except the original FeS_2. The single discharge plateau is likely related to the high discharge current density (53.5 $mA \cdot g^{-1}$) [25,26]. The increased conductivity of Co-doped FeS_2 improved the reactivity, which resulted in the 2nd incomplete charge plateau at 2.46 V because of the low charge potential limit. In addition, as shown in Figure 4, the 1st and 10th discharge curves of DH-7 reveal the lowest charge plateau, which corresponds to the lowest level of polarization and probably accounts for its better electronic conductivity.

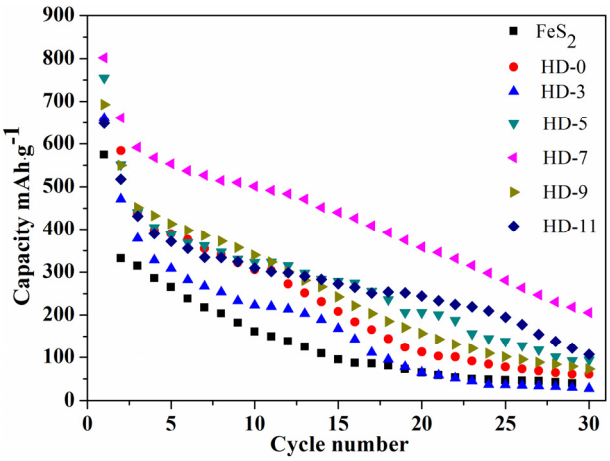

Figure 3. Cycling performance of the samples.

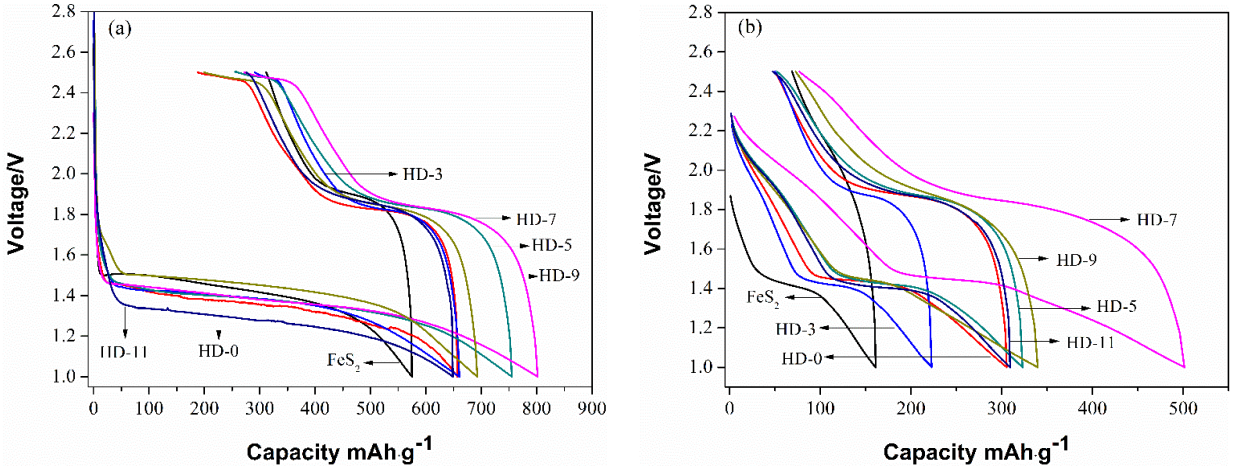

Figure 4. The 1st (**a**) and 10th (**b**) charge-discharge curves of the samples.

EIS measurement was used to investigate the charge transfer resistance, as shown in Figure 5. Meanwhile, the measured impedance data were analyzed using the ZSimpWin software, as listed in Table 1. The Warburg coefficient [27] σ_w is the slope for the function of Z' *vs.* $\omega^{-1/2}$, where ω is the angular frequency in the low-frequency region (Figure 5b). In addition, the diffusion coefficient values of the lithium ions (D_{Li}) [28] and conductivity values (σ) [29] can be determined from Equations (1) and (2), respectively.

$$D_{Li} = 0.5(RT / AF^2\sigma_w C)^2 \quad (1)$$

$$\sigma = t / R_{ct} \cdot A \quad (2)$$

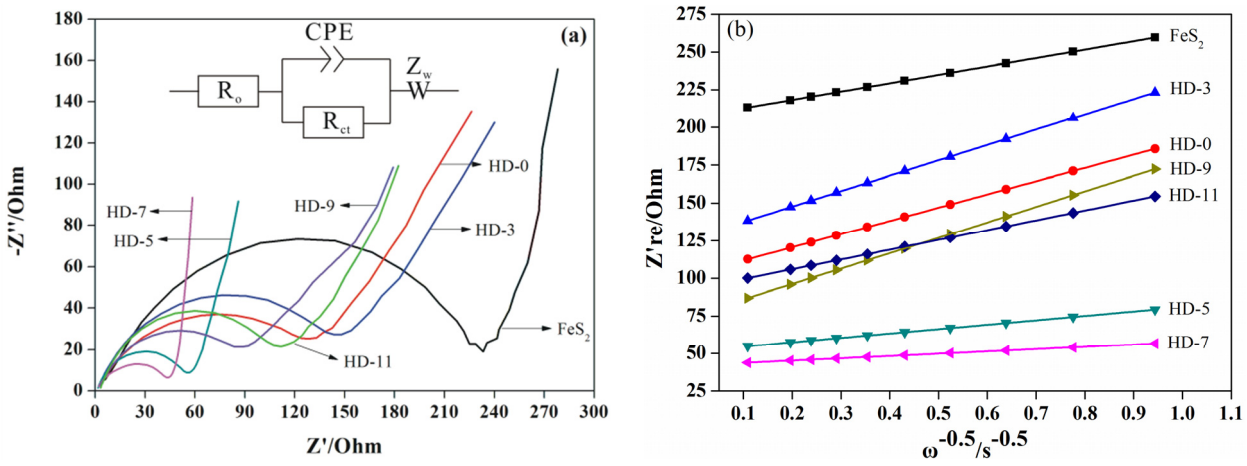

Figure 5. Nyquist plots with the equivalent circuits (**a**) and curves for the functions of *Z'* *vs.* $\omega^{-1/2}$; (**b**) for the samples.

Table 1. Impedance parameters of samples.

Sample	R_{ct} (Ω)	σ_w (Ω·cm²·s$^{-0.5}$)	D_{Li} (cm²·s^{-1})	σ (S·cm^{-1})
FeS_2	234.0	55.6	3.7×10^{-7}	9.7×10^{-6}
DH-0	118.8	176.5	3.6×10^{-8}	1.9×10^{-5}
DH-3	137.5	101.6	1.1×10^{-7}	1.6×10^{-5}
DH-5	52.3	29.3	1.3×10^{-7}	3.3×10^{-5}
DH-7	43.9	15.2	4.9×10^{-6}	5.1×10^{-5}
DH-9	87.9	102.4	1.1×10^{-7}	2.6×10^{-5}
DH-11	105.1	65.1	2.7×10^{-7}	2.2×10^{-5}

Figure 5a displays the Nyquist plots for all samples. The semicircle in the high-frequency range is related to one set of parallel resistor and capacitor [30–32]. As shown in Figure 5 and Table 1, DH-7 had the lowest charge-transfer resistance (R_{ct}) and highest D_{Li}, which suggests the highest activity of electrochemical reactions and fastest migration of lithium ions. These results indicate that DH-7 is the most suitable Co-doped samples for the electrochemical reaction, which is probably the result of better electronic conductivity (Table 1) and specific morphology (Figure 2) of DH-7.

4. Conclusions

In this study, Co-doped FeS_2, which was synthesized using a hydrothermal method, and its electrochemical properties were measured. The results show that the Co element can significantly improve the conductivity and change the morphology of FeS_2. As a result, the electrochemical performance of Co-doped FeS_2 was improved. In particular, the Co-doped sample with 7 wt%, it had the best electrochemical performance with excellent morphology, highest electronic conductivity, and highest migration rate of lithium ions.

Acknowledgments

This work was supported by the National Natural Science Foundation of China (21173198) and the Science and Technology Support Program of Hubei Province, China (2015BCA301).

Author Contributions

All authors contributed equally to this work. Yongchao Liu and Shengping Wang performed experiments and wrote the manuscript.

Conflicts of Interest

The authors declare no conflict of interest.

References

1. Zhang, S.S. The redox mechanism of FeS_2 in non-aqueous electrolytes for lithium and sodium batteries. *J. Mater. Chem. A* **2015**, *3*, 7689–7694.
2. Kirkeminde, A.; Ruzicka, B.A.; Wang, R.; Puna, S.; Zhao, H.; Ren, S. Synthesis and optoelectronic properties of two-dimensional FeS_2 nanoplates. *ACS Appl. Mater. Interfaces* **2012**, *4*, 1174–1177.
3. Cabán-Acevedo, M.; Faber, M.S.; Tan, Y.; Hamers, R.J.; Jin, S. Synthesis and properties of semiconducting iron pyrite (FeS_2) nanowires. *Nano Lett.* **2012**, *12*, 1977–1982.
4. Strauss, E.; Ardel, G.; Livshits, V.; Burstein, L.; Golodnitsky, D.; Peled, E. Lithium polymer electrolyte pyrite rechargeable battery: Comparative characterization of natural pyrite from different sources as cathode material. *J. Power Sources* **2000**, *88*, 206–218.
5. Peled, E.; Golodnitsky, D.; Strauss, E.; Lang, J.; Lavi, Y. Li/CPE/FeS_2 rechargeable battery. *Electrochim. Acta* **1998**, *43*, 1593–1599.
6. Huang, S.; Liu, X.; Li, Q.; Chen, J. Pyrite film synthesized for lithium-ion batteries. *J. Alloy. Compd.* **2009**, *472*, L9–L12.
7. Yersak, T.A.; Macpherson, H.A.; Kim, S.C.; Le, V.-D.; Kang, C.S.; Son, S.-B.; Kim, Y.-H.; Trevey, J.E.; Oh, K.H.; Stoldt, C.; *et al*. Solid state enabled reversible four electron storage. *Adv. Energy Mater.* **2013**, *3*, 120–127.
8. Li, L.; Caban-Acevedo, M.; Girard, S.N.; Jin, S. High-purity iron pyrite (FeS_2) nanowires as high-capacity nanostructured cathodes for lithium-ion batteries. *Nanoscale* **2014**, *6*, 2112–2118.
9. Zhang, D.; Wang, X.; Mai, Y.; Xia, X.; Gu, C.; Tu, J. Enhanced electrochemical performance of FeS_2 synthesized by hydrothermal method for lithium ion batteries. *J. Appl. Electrochem.* **2012**, *42*, 263–269.
10. Huang, L.; Wang, F.; Luan, Z.; Meng, L. Pyrite (FeS_2) thin films deposited by sol-gel method. *Mater. Lett.* **2010**, *64*, 2612–2615.
11. Nakamura, S.; Yamamoto, A. Electrodeposition of pyrite (FeS_2) thin films for photovoltaic cells. *Sol. Energy Mater. Sol. Cells* **2001**, *65*, 79–85.
12. Zhang, D.; Tu, J.P.; Mai, Y.J.; Zhang, J.; Qiao, Y.Q.; Wang, X.L. Preparation and characterization of FeS_2/polyaniline composite electrode in lithium-ion battery. *J. Aust. Ceram. Soc.* **2012**, *48*, 189–193.
13. Choi, Y.J.; Kang, W.G.; Ryu, H.S.; Nam, T.H.; Ahn, H.J.; Cho, K.K.; Kim, K.W.; Ryu, K.S. Effect of Fe addition on cycle performance of FeS_2 cathode for Li/FeS_2 battery. *Mater. Technol.* **2012**, *27*, 124–126.

14. Wang, H.; Wang, Q.; Cheng, Y.; Li, K.; Yao, Y.; Zhang, Q.; Dong, C.; Wang, P.; Schwingenschlögl, U.; Yang, W.; *et al*. Doping monolayer graphene with single atom substitutions. *Nano Lett.* **2011**, *12*, 141–144.
15. Hsiao, S.-C.; Hsu, C.-M.; Chen, S.-Y.; Perng, Y.-H.; Chueh, Y.-L.; Chen, L.-J.; Chou, L.-H. Facile synthesis and characterization of high temperature phase FeS_2 pyrite nanocrystals. *Mater. Lett.* **2012**, *75*, 152–154.
16. Lehner, S.W.; Savage, K.S.; Ayers, J.C. Vapor growth and characterization of pyrite (FeS_2) doped with Co, Ni, and As: Variations in semiconducting properties. *J. Cryst. Growth* **2006**, *286*, 306–317.
17. Diaz-Chao, P.; Ferrer, I.J.; Sanchez, C. Co distribution through n-type pyrite thin films. *Thin Solid Films* **2008**, *516*, 7116–7119.
18. Jiao, J.Q.; Chen, L.P.; Kuang, D.B.; Gao, W.; Feng, H.J.; Xia, J. Synthesis of FeS_2 and Co-doped FeS_2 films with the aid of supercritical carbon dioxide and their photoelectrochemical properties. *RSC Adv.* **2011**, *1*, 255–261.
19. Wang, Q.; Jiao, L.; Han, Y.; Du, H.; Peng, W.; Huan, Q.; Song, D.; Si, Y.; Wang, Y.; Yuan, H. CoS_2 hollow spheres: Fabrication and their application in lithium-ion batteries. *J Phys. Chem. C* **2011**, *115*, 8300–8304.
20. Faber, M.S.; Park, K.; Cabán-Acevedo, M.; Santra, P.K.; Jin, S. Earth-abundant cobalt pyrite (CoS_2) thin film on glass as a robust, high-performance counter electrode for quantum dot-sensitized solar cells. *J. Phys. Chem. Lett.* **2013**, *4*, 1843–1849.
21. Faber, M.S.; Dziedzic, R.; Lukowski, M.A.; Kaiser, N.S.; Ding, Q.; Jin, S. High-performance electrocatalysis using metallic cobalt pyrite (CoS_2) micro- and nanostructures. *J. Am. Chem. Soc.* **2014**, *136*, 10053–10061.
22. Oertel, J.; Ellmer, K.; Bohne, W.; Röhrich, J.; Tributsch, H. Growth of n-type polycrystalline pyrite (FeS_2) films by metalorganic chemical vapour deposition and their electrical characterization. *J. Cryst. Growth* **1999**, *198–199*, 1205–1210.
23. Wang, F.; Huang, L.; Luan, Z.; Huang, J.; Meng, L. Effect of sulfurization temperature on the surface roughening, electrical and optical properties of FeS_2 films deposited by sol-gel method. *Mater. Chem. Phys.* **2012**, *132*, 505–508.
24. Gong, M.G.; Kirkeminde, A.; Ren, S.Q. Symmetry-defying iron pyrite (FeS_2) nanocrystals through oriented attachment. *Sci. Rep.* **2013**, *3*, doi:10.1038/srep02092.
25. Fong, R.; Dahn, J.R.; Jones, C.H.W. Electrochemistry of pyrite-based cathodes for ambient-temperature lithium batteries. *J. Electrochem. Soc.* **1989**, *136*, 3206–3210.
26. Shao-Horn, Y.; Horn, Q.C. Chemical, structural and electrochemical comparison of natural and synthetic FeS_2 pyrite in lithium cells. *Electrochim. Acta* **2001**, *46*, 2613–2621.
27. Bao, W.; Zhuang, Q.; Xu, S.; Cui, Y.; Shi, Y.; Qiang, Y. Investigation of electronic and ionic transport properties in α-MoO_3 cathode material by electrochemical impedance spectroscopy. *Ionics* **2013**, *19*, 1005–1013.
28. Cui, Y.; Zhao, X.; Guo, R. Improved electrochemical performance of $La_{0.7}Sr_{0.3}MnO_3$ and carbon co-coated $LiFePO_4$ synthesized by freeze-drying process. *Electrochim. Acta* **2010**, *55*, 922–926.
29. Subba Reddy, C.V.; Chen, M.; Jin, W.; Zhu, Q.Y.; Chen, W.; Mho, S.-I. Characterization of (PVDF + $LiFePO_4$) solid polymer electrolyte. *J. Appl. Electrochem.* **2007**, *37*, 637–642.

30. Moya, A.A. Electrochemical impedance of ion-exchange systems with weakly charged membranes. *Ionics* **2013**, *19*, 1271–1283.
31. Schmidt, J.P.; Chrobak, T.; Ender, M.; Illig, J.; Klotz, D.; Ivers-Tiffée, E. Studies on $LiFePO_4$ as cathode material using impedance spectroscopy. *J. Power Sources* **2011**, *196*, 5342–5348.
32. Andre, D.; Meiler, M.; Steiner, K.; Walz, H.; Soczka-Guth, T.; Sauer, D.U. Characterization of high-power lithium-ion batteries by electrochemical impedance spectroscopy. II: Modelling. *J. Power Sources* **2011**, *196*, 5349–5356.